Measurement of the Inclusive Jet Cross Section in $p\bar{p}$ Interactions at $\sqrt{s} = 1.96$ TeV Using a Cone-based Jet Algorithm

A. Abulencia,[23] D. Acosta,[17] J. Adelman,[13] T. Affolder,[10] T. Akimoto,[53] M.G. Albrow,[16] D. Ambrose,[16] S. Amerio,[42] D. Amidei,[33] A. Anastassov,[50] K. Anikeev,[16] A. Annovi,[44] J. Antos,[1] M. Aoki,[53] G. Apollinari,[16] J.-F. Arguin,[32] T. Arisawa,[55] A. Artikov,[14] W. Ashmanskas,[16] A. Attal,[8] F. Azfar,[41] P. Azzi-Bacchetta,[42] P. Azzurri,[44] N. Bacchetta,[42] H. Bachacou,[28] W. Badgett,[16] A. Barbaro-Galtieri,[28] V.E. Barnes,[46] B.A. Barnett,[24] S. Baroiant,[7] V. Bartsch,[30] G. Bauer,[31] F. Bedeschi,[44] S. Behari,[24] S. Belforte,[52] G. Bellettini,[44] J. Bellinger,[57] A. Belloni,[31] E. Ben-Haim,[16] D. Benjamin,[15] A. Beretvas,[16] J. Beringer,[28] T. Berry,[29] A. Bhatti,[48] M. Binkley,[16] D. Bisello,[42] M. Bishai,[16] R. E. Blair,[2] C. Blocker,[6] K. Bloom,[33] B. Blumenfeld,[24] A. Bocci,[48] A. Bodek,[47] V. Boisvert,[47] G. Bolla,[46] A. Bolshov,[31] D. Bortoletto,[46] J. Boudreau,[45] S. Bourov,[16] A. Boveia,[10] B. Brau,[10] C. Bromberg,[34] E. Brubaker,[13] J. Budagov,[14] H.S. Budd,[47] S. Budd,[23] K. Burkett,[16] G. Busetto,[42] P. Bussey,[20] K. L. Byrum,[2] S. Cabrera,[15] M. Campanelli,[19] M. Campbell,[33] F. Canelli,[8] A. Canepa,[46] D. Carlsmith,[57] R. Carosi,[44] S. Carron,[15] M. Casarsa,[52] A. Castro,[5] P. Catastini,[44] D. Cauz,[52] M. Cavalli-Sforza,[3] A. Cerri,[28] L. Cerrito,[41] S.H. Chang,[27] J. Chapman,[33] Y.C. Chen,[1] M. Chertok,[7] G. Chiarelli,[44] G. Chlachidze,[14] F. Chlebana,[16] I. Cho,[27] K. Cho,[27] D. Chokheli,[14] J.P. Chou,[21] P.H. Chu,[23] S.H. Chuang,[57] K. Chung,[12] W.H. Chung,[57] Y.S. Chung,[47] M. Ciljak,[44] C.I. Ciobanu,[23] M.A. Ciocci,[44] A. Clark,[19] D. Clark,[6] M. Coca,[15] A. Connolly,[28] M.E. Convery,[48] J. Conway,[7] B. Cooper,[30] K. Copic,[33] M. Cordelli,[18] G. Cortiana,[42] A. Cruz,[17] J. Cuevas,[11] R. Culbertson,[16] D. Cyr,[57] S. DaRonco,[42] S. D'Auria,[20] M. D'onofrio,[19] D. Dagenhart,[6] P. de Barbaro,[47] S. De Cecco,[49] A. Deisher,[28] G. De Lentdecker,[47] M. Dell'Orso,[44] S. Demers,[47] L. Demortier,[48] J. Deng,[15] M. Deninno,[5] D. De Pedis,[49] P.F. Derwent,[16] C. Dionisi,[49] J.R. Dittmann,[4] P. DiTuro,[50] C. Dörr,[25] A. Dominguez,[28] S. Donati,[44] M. Donega,[19] P. Dong,[8] J. Donini,[42] T. Dorigo,[42] S. Dube,[50] K. Ebina,[55] J. Efron,[38] J. Ehlers,[19] R. Erbacher,[7] D. Errede,[23] S. Errede,[23] R. Eusebi,[47] H.C. Fang,[28] S. Farrington,[29] I. Fedorko,[44] W.T. Fedorko,[13] R.G. Feild,[58] M. Feindt,[25] J.P. Fernandez,[46] R. Field,[17] G. Flanagan,[34] L.R. Flores-Castillo,[45] A. Foland,[21] S. Forrester,[7] G.W. Foster,[16] M. Franklin,[21] J.C. Freeman,[28] Y. Fujii,[26] I. Furic,[13] A. Gajjar,[29] M. Gallinaro,[48] J. Galyardt,[12] J.E. Garcia,[44] M. Garcia Sciveres,[28] A.F. Garfinkel,[46] C. Gay,[58] H. Gerberich,[23] E. Gerchtein,[12] D. Gerdes,[33] S. Giagu,[49] P. Giannetti,[44] A. Gibson,[28] K. Gibson,[12] C. Ginsburg,[16] K. Giolo,[46] M. Giordani,[52] M. Giunta,[44] G. Giurgiu,[12] V. Glagolev,[14] D. Glenzinski,[16] M. Gold,[36] N. Goldschmidt,[33] J. Goldstein,[41] G. Gomez,[11] G. Gomez-Ceballos,[11] M. Goncharov,[51] O. González,[46] I. Gorelov,[36] A.T. Goshaw,[15] Y. Gotra,[45] K. Goulianos,[48] A. Gresele,[42] M. Griffiths,[29] S. Grinstein,[21] C. Grosso-Pilcher,[13] U. Grundler,[23] J. Guimaraes da Costa,[21] C. Haber,[28] S.R. Hahn,[16] K. Hahn,[43] E. Halkiadakis,[47] A. Hamilton,[32] B.-Y. Han,[47] R. Handler,[57] F. Happacher,[18] K. Hara,[53] M. Hare,[54] S. Harper,[41] R.F. Harr,[56] R.M. Harris,[16] K. Hatakeyama,[48] J. Hauser,[8] C. Hays,[15] H. Hayward,[29] A. Heijboer,[43] B. Heinemann,[29] J. Heinrich,[43] M. Hennecke,[25] M. Herndon,[57] J. Heuser,[25] D. Hidas,[15] C.S. Hill,[10] D. Hirschbuehl,[25] A. Hocker,[16] A. Holloway,[21] S. Hou,[1] M. Houlden,[29] S.-C. Hsu,[9] B.T. Huffman,[41] R.E. Hughes,[38] J. Huston,[34] K. Ikado,[55] J. Incandela,[10] G. Introzzi,[44] M. Iori,[49] Y. Ishizawa,[53] A. Ivanov,[7] B. Iyutin,[31] E. James,[16] D. Jang,[50] B. Jayatilaka,[33] D. Jeans,[49] H. Jensen,[16] E.J. Jeon,[27] M. Jones,[46] K.K. Joo,[27] S.Y. Jun,[12] T.R. Junk,[23] T. Kamon,[51] J. Kang,[33] M. Karagoz-Unel,[37] P.E. Karchin,[56] Y. Kato,[40] Y. Kemp,[25] R. Kephart,[16] U. Kerzel,[25] V. Khotilovich,[51] B. Kilminster,[38] D.H. Kim,[27] H.S. Kim,[27] J.E. Kim,[27] M.J. Kim,[12] M.S. Kim,[27] S.B. Kim,[27] S.H. Kim,[53] Y.K. Kim,[13] M. Kirby,[15] L. Kirsch,[6] S. Klimenko,[17] M. Klute,[31] B. Knuteson,[31] B.R. Ko,[15] H. Kobayashi,[53] K. Kondo,[55] D.J. Kong,[27] J. Konigsberg,[17] K. Kordas,[18] A. Korytov,[17] A.V. Kotwal,[15] A. Kovalev,[43] J. Kraus,[23] I. Kravchenko,[31] M. Kreps,[25] A. Kreymer,[16] J. Kroll,[43] N. Krumnack,[4] M. Kruse,[15] V. Krutelyov,[51] S. E. Kuhlmann,[2] Y. Kusakabe,[55] S. Kwang,[13] A.T. Laasanen,[46] S. Lai,[32] S. Lami,[44] S. Lammel,[16] M. Lancaster,[30] R.L. Lander,[7] K. Lannon,[38] A. Lath,[50] G. Latino,[44] I. Lazzizzera,[42] C. Lecci,[25] T. LeCompte,[2] J. Lee,[47] J. Lee,[27] S.W. Lee,[51] R. Lefèvre,[3] N. Leonardo,[31] S. Leone,[44] S. Levy,[13] J.D. Lewis,[16] K. Li,[58] C. Lin,[58] C.S. Lin,[16] M. Lindgren,[16] E. Lipeles,[9] T.M. Liss,[23] A. Lister,[19] D.O. Litvintsev,[16] T. Liu,[16] Y. Liu,[19] N.S. Lockyer,[43] A. Loginov,[35] M. Loreti,[42] P. Loverre,[49] R.-S. Lu,[1] D. Lucchesi,[42] P. Lujan,[28] P. Lukens,[16] G. Lungu,[17] L. Lyons,[41] J. Lys,[28] R. Lysak,[1] E. Lytken,[46] P. Mack,[25] D. MacQueen,[32] R. Madrak,[16] K. Maeshima,[16] P. Maksimovic,[24] G. Manca,[29] F. Margaroli,[5] R. Marginean,[16] C. Marino,[23] A. Martin,[58] M. Martin,[24] V. Martin,[37] M. Martínez,[3] T. Maruyama,[53] H. Matsunaga,[53] M.E. Mattson,[56] R. Mazini,[32] P. Mazzanti,[5] K.S. McFarland,[47] D. McGivern,[30] P. McIntyre,[51] P. McNamara,[50] R. McNulty,[29] A. Mehta,[29] S. Menzemer,[31] A. Menzione,[44] P. Merkel,[46] C. Mesropian,[48]

A. Messina,[49] M. von der Mey,[8] T. Miao,[16] N. Miladinovic,[6] J. Miles,[31] R. Miller,[34] J.S. Miller,[33] C. Mills,[10] M. Milnik,[25] R. Miquel,[28] S. Miscetti,[18] G. Mitselmakher,[17] A. Miyamoto,[26] N. Moggi,[5] B. Mohr,[8] R. Moore,[16] M. Morello,[44] P. Movilla Fernandez,[28] J. Mülmenstädt,[28] A. Mukherjee,[16] M. Mulhearn,[31] Th. Muller,[25] R. Mumford,[24] P. Murat,[16] J. Nachtman,[16] S. Nahn,[58] I. Nakano,[39] A. Napier,[54] D. Naumov,[36] V. Necula,[17] C. Neu,[43] M.S. Neubauer,[9] J. Nielsen,[28] T. Nigmanov,[45] L. Nodulman,[2] O. Norniella,[3] T. Ogawa,[55] S.H. Oh,[15] Y.D. Oh,[27] T. Okusawa,[40] R. Oldeman,[29] R. Orava,[22] K. Osterberg,[22] C. Pagliarone,[44] E. Palencia,[11] R. Paoletti,[44] V. Papadimitriou,[16] A. Papikonomou,[25] A.A. Paramonov,[13] B. Parks,[38] S. Pashapour,[32] J. Patrick,[16] G. Pauletta,[52] M. Paulini,[12] C. Paus,[31] D.E. Pellett,[7] A. Penzo,[52] T.J. Phillips,[15] G. Piacentino,[44] J. Piedra,[11] K. Pitts,[23] C. Plager,[8] L. Pondrom,[57] G. Pope,[45] X. Portell,[3] O. Poukhov,[14] N. Pounder,[41] F. Prakoshyn,[14] A. Pronko,[16] J. Proudfoot,[2] F. Ptohos,[18] G. Punzi,[44] J. Pursley,[24] J. Rademacker,[41] A. Rahaman,[45] A. Rakitin,[31] S. Rappoccio,[21] F. Ratnikov,[50] B. Reisert,[16] V. Rekovic,[36] N. van Remortel,[22] P. Renton,[41] M. Rescigno,[49] S. Richter,[25] F. Rimondi,[5] K. Rinnert,[25] L. Ristori,[44] W.J. Robertson,[15] A. Robson,[20] T. Rodrigo,[11] E. Rogers,[23] S. Rolli,[54] R. Roser,[16] M. Rossi,[52] R. Rossin,[17] C. Rott,[46] A. Ruiz,[11] J. Russ,[12] V. Rusu,[13] D. Ryan,[54] H. Saarikko,[22] S. Sabik,[32] A. Safonov,[7] W.K. Sakumoto,[47] G. Salamanna,[49] O. Salto,[3] D. Saltzberg,[8] C. Sanchez,[3] L. Santi,[52] S. Sarkar,[49] K. Sato,[53] P. Savard,[32] A. Savoy-Navarro,[16] T. Scheidle,[25] P. Schlabach,[16] E.E. Schmidt,[16] M.P. Schmidt,[58] M. Schmitt,[37] T. Schwarz,[33] L. Scodellaro,[11] A.L. Scott,[10] A. Scribano,[44] F. Scuri,[44] A. Sedov,[46] S. Seidel,[36] Y. Seiya,[40] A. Semenov,[14] F. Semeria,[5] L. Sexton-Kennedy,[16] I. Sfiligoi,[18] M.D. Shapiro,[28] T. Shears,[29] P.F. Shepard,[45] D. Sherman,[21] M. Shimojima,[53] M. Shochet,[13] Y. Shon,[57] I. Shreyber,[35] A. Sidoti,[44] A. Sill,[16] P. Sinervo,[32] A. Sisakyan,[14] J. Sjolin,[41] A. Skiba,[25] A.J. Slaughter,[16] K. Sliwa,[54] D. Smirnov,[36] J. R. Smith,[7] F.D. Snider,[16] R. Snihur,[32] M. Soderberg,[33] A. Soha,[7] S. Somalwar,[50] V. Sorin,[34] J. Spalding,[16] F. Spinella,[44] P. Squillacioti,[44] M. Stanitzki,[58] A. Staveris-Polykalas,[44] R. St. Denis,[20] B. Stelzer,[8] O. Stelzer-Chilton,[32] D. Stentz,[37] J. Strologas,[36] D. Stuart,[10] J.S. Suh,[27] A. Sukhanov,[17] K. Sumorok,[31] H. Sun,[54] T. Suzuki,[53] A. Taffard,[23] R. Tafirout,[32] R. Takashima,[39] Y. Takeuchi,[53] K. Takikawa,[53] M. Tanaka,[2] R. Tanaka,[39] M. Tecchio,[33] P.K. Teng,[1] K. Terashi,[48] S. Tether,[31] J. Thom,[16] A.S. Thompson,[20] E. Thomson,[43] P. Tipton,[47] V. Tiwari,[12] S. Tkaczyk,[16] D. Toback,[51] K. Tollefson,[34] T. Tomura,[53] D. Tonelli,[44] M. Tönnesmann,[34] S. Torre,[44] D. Torretta,[16] S. Tourneur,[16] W. Trischuk,[32] R. Tsuchiya,[55] S. Tsuno,[39] N. Turini,[44] F. Ukegawa,[53] T. Unverhau,[20] S. Uozumi,[53] D. Usynin,[43] L. Vacavant,[28] A. Vaiciulis,[47] S. Vallecorsa,[19] A. Varganov,[33] E. Vataga,[36] G. Velev,[16] G. Veramendi,[23] V. Veszpremi,[46] T. Vickey,[23] R. Vidal,[16] I. Vila,[11] R. Vilar,[11] I. Vollrath,[32] I. Volobouev,[28] F. Würthwein,[9] P. Wagner,[51] R. G. Wagner,[2] R.L. Wagner,[16] W. Wagner,[25] R. Wallny,[8] T. Walter,[25] Z. Wan,[50] M.J. Wang,[1] S.M. Wang,[17] A. Warburton,[32] B. Ward,[20] S. Waschke,[20] D. Waters,[30] T. Watts,[50] M. Weber,[28] W.C. Wester III,[16] B. Whitehouse,[54] D. Whiteson,[43] A.B. Wicklund,[2] E. Wicklund,[16] H.H. Williams,[43] P. Wilson,[16] B.L. Winer,[38] P. Wittich,[43] S. Wolbers,[16] C. Wolfe,[13] S. Worm,[50] T. Wright,[33] X. Wu,[19] S.M. Wynne,[29] A. Yagil,[16] K. Yamamoto,[40] J. Yamaoka,[50] Y. Yamashita.,[39] C. Yang,[58] U.K. Yang,[13] W.M. Yao,[28] G.P. Yeh,[16] J. Yoh,[16] K. Yorita,[13] T. Yoshida,[40] I. Yu,[27] S.S. Yu,[43] J.C. Yun,[16] L. Zanello,[49] A. Zanetti,[52] I. Zaw,[21] F. Zetti,[44] X. Zhang,[23] J. Zhou,[50] and S. Zucchelli[5]

(CDF Collaboration)

[1]*Institute of Physics, Academia Sinica, Taipei, Taiwan 11529, Republic of China*
[2]*Argonne National Laboratory, Argonne, Illinois 60439*
[3]*Institut de Fisica d'Altes Energies, Universitat Autonoma de Barcelona, E-08193, Bellaterra (Barcelona), Spain*
[4]*Baylor University, Waco, Texas 76798*
[5]*Istituto Nazionale di Fisica Nucleare, University of Bologna, I-40127 Bologna, Italy*
[6]*Brandeis University, Waltham, Massachusetts 02254*
[7]*University of California, Davis, Davis, California 95616*
[8]*University of California, Los Angeles, Los Angeles, California 90024*
[9]*University of California, San Diego, La Jolla, California 92093*
[10]*University of California, Santa Barbara, Santa Barbara, California 93106*
[11]*Instituto de Fisica de Cantabria, CSIC-University of Cantabria, 39005 Santander, Spain*
[12]*Carnegie Mellon University, Pittsburgh, PA 15213*
[13]*Enrico Fermi Institute, University of Chicago, Chicago, Illinois 60637*
[14]*Joint Institute for Nuclear Research, RU-141980 Dubna, Russia*
[15]*Duke University, Durham, North Carolina 27708*
[16]*Fermi National Accelerator Laboratory, Batavia, Illinois 60510*
[17]*University of Florida, Gainesville, Florida 32611*
[18]*Laboratori Nazionali di Frascati, Istituto Nazionale di Fisica Nucleare, I-00044 Frascati, Italy*
[19]*University of Geneva, CH-1211 Geneva 4, Switzerland*

[20]Glasgow University, Glasgow G12 8QQ, United Kingdom
[21]Harvard University, Cambridge, Massachusetts 02138
[22]Division of High Energy Physics, Department of Physics, University of Helsinki and Helsinki Institute of Physics, FIN-00014, Helsinki, Finland
[23]University of Illinois, Urbana, Illinois 61801
[24]The Johns Hopkins University, Baltimore, Maryland 21218
[25]Institut für Experimentelle Kernphysik, Universität Karlsruhe, 76128 Karlsruhe, Germany
[26]High Energy Accelerator Research Organization (KEK), Tsukuba, Ibaraki 305, Japan
[27]Center for High Energy Physics: Kyungpook National University, Taegu 702-701; Seoul National University, Seoul 151-742; and SungKyunKwan University, Suwon 440-746; Korea
[28]Ernest Orlando Lawrence Berkeley National Laboratory, Berkeley, California 94720
[29]University of Liverpool, Liverpool L69 7ZE, United Kingdom
[30]University College London, London WC1E 6BT, United Kingdom
[31]Massachusetts Institute of Technology, Cambridge, Massachusetts 02139
[32]Institute of Particle Physics: McGill University, Montréal, Canada H3A 2T8; and University of Toronto, Toronto, Canada M5S 1A7
[33]University of Michigan, Ann Arbor, Michigan 48109
[34]Michigan State University, East Lansing, Michigan 48824
[35]Institution for Theoretical and Experimental Physics, ITEP, Moscow 117259, Russia
[36]University of New Mexico, Albuquerque, New Mexico 87131
[37]Northwestern University, Evanston, Illinois 60208
[38]The Ohio State University, Columbus, Ohio 43210
[39]Okayama University, Okayama 700-8530, Japan
[40]Osaka City University, Osaka 588, Japan
[41]University of Oxford, Oxford OX1 3RH, United Kingdom
[42]University of Padova, Istituto Nazionale di Fisica Nucleare, Sezione di Padova-Trento, I-35131 Padova, Italy
[43]University of Pennsylvania, Philadelphia, Pennsylvania 19104
[44]Istituto Nazionale di Fisica Nucleare Pisa, Universities of Pisa, Siena and Scuola Normale Superiore, I-56127 Pisa, Italy
[45]University of Pittsburgh, Pittsburgh, Pennsylvania 15260
[46]Purdue University, West Lafayette, Indiana 47907
[47]University of Rochester, Rochester, New York 14627
[48]The Rockefeller University, New York, New York 10021
[49]Istituto Nazionale di Fisica Nucleare, Sezione di Roma 1, University of Rome "La Sapienza," I-00185 Roma, Italy
[50]Rutgers University, Piscataway, New Jersey 08855
[51]Texas A&M University, College Station, Texas 77843
[52]Istituto Nazionale di Fisica Nucleare, University of Trieste/ Udine, Italy
[53]University of Tsukuba, Tsukuba, Ibaraki 305, Japan
[54]Tufts University, Medford, Massachusetts 02155
[55]Waseda University, Tokyo 169, Japan
[56]Wayne State University, Detroit, Michigan 48201
[57]University of Wisconsin, Madison, Wisconsin 53706
[58]Yale University, New Haven, Connecticut 06520

(Dated: October 27, 2005)

We present a measurement of the inclusive jet cross section in $p\bar{p}$ interactions at $\sqrt{s} = 1.96$ TeV using 385 pb^{-1} of data collected with the CDF II detector at the Fermilab Tevatron. The results are obtained using an improved cone-based jet algorithm (Midpoint). The data cover the jet transverse momentum range from 61 to 620 GeV/c, extending the reach by almost 150 GeV/c compared with previous measurements at the Tevatron. The results are in good agreement with next-to-leading order perturbative QCD predictions using the CTEQ6.1M parton distribution functions.

PACS numbers: 13.87.Ce, 12.38.Qk, 13.85.Ni

The differential jet production cross section at the Tevatron probes the world's highest momentum transfers in particle collisions, is potentially sensitive to a wide variety of new physics, such as quark compositeness, and tests perturbative QCD (pQCD) over more than eight orders of magnitude. There was great interest when the inclusive jet cross section measured by the CDF collaboration at the center of mass energy $\sqrt{s} = 1.8$ TeV [1, 2] exhibited an excess in the high transverse energy E_T region when compared to next-to-leading order (NLO) QCD predictions obtained using then-current parton distribution functions (PDFs) [3]. Global PDF analysis by

CTEQ [4, 5] demonstrated that the excess could be explained by an enhanced gluon distribution at large momentum fraction x. Recent global PDF fits (CTEQ6, CTEQ6.1, MRST2004) [6–8], which include the Run I Tevatron jet data [1, 9], find an increased gluon density at high x and provide a good description of the Run I Tevatron data. The gluon distribution is still poorly constrained in this x region and contributes significantly to the theoretical uncertainty for many interesting processes at the Tevatron and the LHC. The increase in $\sqrt{s}$ from 1.8 to 1.96 TeV, together with higher luminosity in Run II, allow more precise jet production measurements with a significantly extended kinematic range.

Jet algorithms cluster together partons, particles or calorimeter towers that have small transverse momenta relative to a jet axis (the k_T algorithm) or are nearby in angle (the cone algorithm). In this letter, we report the results of an inclusive jet measurement using a cone algorithm for the rapidity region $0.1 < |y| < 0.7$ [10]. The analysis is described in greater detail in Ref. [11]. We use the Midpoint algorithm, an improved iterative cone clustering algorithm [12]. It is difficult to use previous iterative cone algorithms [2, 9] with higher order pQCD calculations due to the presence of infrared singularities. The Midpoint algorithm places additional seeds (directions for jet cones) between stable cones having a separation of less than twice the size of the clustering cones; the use of these additional seeds removes the problem with infrared singularities. The Midpoint algorithm uses four-vector kinematics for clustering individual partons, particles or calorimeter towers and jets are described using rapidity (y) and transverse momentum (p_T); the CDF Run I jet clustering algorithm used scalar summation for clustering, pseudorapidity (η) [10], and the transverse energy (E_T) as described in [13].

The CDF II detector is a magnetic spectrometer which is described in detail elsewhere [14]. Here we describe briefly those components that are crucial to this measurement. The central detector consists of a silicon vertex detector inside a cylindrical drift chamber. Surrounding the tracking detectors is a superconducting solenoid which provides a 1.4 T magnetic field. Outside the solenoid is the central calorimeter, divided into electromagnetic (CEM) and hadronic (CHA) sections. The central calorimeter consists of 48 modules, segmented into towers of granularity $\Delta\eta \times \Delta\phi \approx 0.1 \times 0.26$, and covers a pseudorapidity range up to 1.1. The CEM is a lead-scintillator calorimeter; the CHA is an iron-scintillator calorimeter with a depth of approximately 4.7 interaction lengths. The energy resolution of the CEM for electrons is $\sigma(E_T)/E_T = 13.5\%/\sqrt{E_T(\mathrm{GeV})} \oplus 2\%$ while the average energy resolution of the CHA for charged pions is $\sigma(E_T)/E_T = 50\%/\sqrt{E_T(\mathrm{GeV})} \oplus 3\%$. The forward region, $1.1 < |\eta| < 3.6$, is covered by the "Plug Calorimeters" consisting of lead-scintillator for the electromagnetic section and iron-scintillator for the hadronic section. The region between the central and forward calorimeters, $0.7 < |\eta| < 1.3$, is covered by an iron-scintillator hadron calorimeter with similar segmentation to the central calorimeter.

This measurement uses a data sample corresponding to an integrated luminosity of 385 pb^{-1} collected between February 2002 and August 2004. The data were collected using four trigger paths. The Level 1 trigger requires a calorimeter trigger tower, consisting of two calorimeter towers adjacent in η, to have either $E_T > 5$ GeV or $E_T > 10$ GeV. At Level 2, the calorimeter towers are clustered using a nearest neighbor algorithm. Four trigger paths with cluster $E_T > 15$, 40, 60, and 90 GeV are used. Events in these paths are required to pass jet $E_T > 20$ (J20), 50 (J50), 70 (J70) and 100 (J100) GeV thresholds at Level 3, where the clustering is performed using a cone algorithm with a cone radius $R_{cone} = 0.7$.

Cosmic ray events are rejected by a cut on the missing transverse energy ($\not{E}_T$) significance, defined as $\not{E}_T/\sqrt{\Sigma E_T}$, where $\not{E}_T$ and ΣE_T are the magnitude of the vector sum and the scalar sum of E_T in all calorimeter towers with $E_T > 100$ MeV. For J20, J50, J70 and J100 we remove events having a $\not{E}_T$ significance greater than 3.5, 5, 5 and 6 GeV$^{1/2}$ respectively. In addition, all events containing jets with $p_T > 360$ GeV$/c$ and passing the analysis cuts were visually scanned, and no cosmic ray events were found. In order to ensure that the jet energy is well measured, the event vertex is required to be within 60 cm of the center of the detector along the beam direction. The efficiency for this cut is determined to be 95% from the beam profile measured using a minimum bias sample. Jets are required to have a rapidity $|y|$ between 0.1 and 0.7 to reduce the effects of the gap at $z = 0$ between calorimeter modules and at the transition region between the central and plug calorimeters. Jets in this rapidity region are measured with a RMS resolution of approximately 12

There are two essential stages for any jet algorithm. First, the objects (partons, particles or calorimeter towers) belonging to a cluster are identified. Second, the kinematic variables defining the jet are calculated from the objects comprising a cluster. The Midpoint algorithm makes use of 4-vectors throughout the clustering process. The detector towers are sorted in order of descending p_T. Only towers passing a seed cut, $p_T^{tower} > p_T^{seed}$, are used as starting points for the initial jet cones. The seed threshold is chosen to be 1 GeV$/c$; its value has a negligible effect on jets in the kinematic region used in this measurement. A tower passing the threshold of 100 MeV$/c$ is clustered into a cone and eventually into a jet if the separation from the axis of the cone in (y, ϕ) is smaller than the cone's radius. There is no threshold for particle and parton clustering. For this measurement, we use a cone radius of 0.7 defined in (y, ϕ) space.

After each iteration the jet centroid position is updated. The jet clustering is repeated until all of the jet cones are stable. A cone is stable when the tower list is unchanged from the previous iteration. After all stable cones have been determined, an additional seed is defined at the midpoint between any two cones separated by less than twice the clustering radius, and the process is repeated. After this stage two overlapping cones, if present, are merged into a single jet if the shared energy is $> 75\%$ of the energy of the jet with lower p_T; otherwise the shared towers are assigned to the nearest jet. This splitting/merging procedure is iterated until the tower assignments to jets are stable. The jet kinematic properties are defined as (4-vector recombination scheme):

$$\begin{aligned} p^{jet} &= (E^{jet}, \mathbf{p}^{jet}) = \sum_{i \subset J=c} (E^i, p^i_x, p^i_y, p^i_z), \\ p_T^{jet} &= \sqrt{(p_x^{jet})^2 + (p_y^{jet})^2}, \\ y^{jet} &= \frac{1}{2} \ln \left(\frac{E^{jet} + p_z^{jet}}{E^{jet} - p_z^{jet}} \right), \\ \phi^{jet} &= \tan^{-1} \left(\frac{p_y^{jet}}{p_x^{jet}} \right). \end{aligned} \tag{1}$$

The inclusive differential jet cross section is defined as:

$$\frac{d^2\sigma}{dp_T dy} = \frac{1}{\Delta y} \frac{1}{\int L dt} \frac{N_{jet}/\epsilon}{\Delta p_T}, \tag{2}$$

where N_{jet} is the number of jets in the p_T range, Δp_T, ϵ is the trigger and vertex correction efficiency, $\int Ldt$ is the effective integrated luminosity, and $\Delta y = 1.2$ is the rapidity interval used in the analysis. A trigger efficiency greater than 99.5% is required to include the jets collected by a given trigger threshold. The measured calorimeter-level jet cross section must be corrected for detector effects and for energy from additional $p\bar{p}$ interactions in the same bunch crossing (pile-up). For this sample, the average number of additional $p\bar{p}$ interactions is about 0.9. The pile-up corrections subtract 0.93($\pm$0.14) GeV/c for each additional primary vertex from the measured jet p_T [17].

The detector response corrections are determined from a detector simulation and a jet fragmentation model. The detector response is determined using a GEANT-based detector simulation [15] in which a parametrized shower simulation (GFLASH [16]) is used for the calorimeter simulation. The GFLASH parameters are tuned to test beam data for electrons and high-p_T charged pions and to the collision data for low-p_T charged hadrons [17]. PYTHIA 6.216 [18], with Tune A [19], is used for the production and fragmentation of the jets. Tune A refers to the values of the parameters describing multiple-parton interactions and initial state radiation which have been adjusted to reproduce the energy observed in the region transverse to the leading jet in the data from Run I. It has been shown to provide a reasonable description of the measured energy distribution inside a jet [20].

The measured p_T spectrum must be corrected for detector effects before it can be compared to theoretical predictions. We cluster the final state stable particles [21] in PYTHIA using the same algorithm as the one used to cluster calorimeter towers. The resulting jets contains all the particles from the $p\bar{p}$ collision, including those from the hard scatter, multiple parton-parton interactions and beam remnants. The correction, done in two correlated steps, is determined from a large sample of PYTHIA events, passed through the CDF detector simulation. First, a p_T-dependent correction is determined by matching the particle jet to the corresponding calorimeter jet and is applied to each measured jet. A binned spectrum is formed from the corrected p_T of each jet. The bin widths are chosen to commensurate jet energy resolution and statistics. The p_T correction ranges from 1.17 at 65 GeV/c to 1.04 at 550 GeV/c. The spectrum must be further corrected for bin-to-bin jet migration due to the finite energy resolution of the calorimeter. This unfolding correction depends on the detector energy resolution and the true spectrum as well as the p_T-dependent correction that was applied in the first step. The PYTHIA events are reweighted to match the experimental spectrum before the correction factors are calculated. A bin-by-bin unfolding correction is then determined by taking the ratio of the binned hadron level cross section and calorimeter level cross section corrected by the p_T-dependent correction. The size of the smearing correction varies from 1.26 at $p_T = 65$ GeV/c to 2.36 at $p_T = 550$ GeV/c. The applied corrections remove the detector effects from the raw cross section and the corrected hadron level cross section can now be compared to theoretical predictions.

The main systematic uncertainties on the measured inclusive jet cross section arise from four sources: the jet energy scale, the jet energy resolution, the unfolding of the measured cross section to the hadron level cross section and the luminosity. The dominant source of uncertainty is from the jet energy scale. The energy scale is known to better than 3% over the entire transverse momentum range, leading to an uncertainty on the jet cross section varying from 10% at low p_T to 60% at high p_T. This is better than the uncertainty achieved by CDF in Run I. The luminosity uncertainty is 6%, independent of p_T and is not included in the quoted systematic error. Other effects considered were determined to have a negligible effect on the cross section. The total experimental systematic uncertainty on the inclusive jet cross section varies from approximately 15% at $p_T = 65$ GeV/c to 59% at $p_T = 550$ GeV/c.

To compare the data with predictions for jets of partons as obtained from NLO calculations, the data must be further corrected for underlying event and hadronization effects. For the former, we correct for the energy in the jet cone not associated with the hard scatter, i.e., from the collisions of other partons in the proton and antiproton. The latter corrects for particles outside the jet cone originating from partons whose trajectories lie inside the jet cone. It does not correct for the effects of hard gluon emission outside the jet cone, which are already accounted for in the NLO prediction. The bin-by-bin hadron-to-parton corrections are obtained by applying the Midpoint clustering algorithm to the hadron level and to the parton level outputs of the PYTHIA Tune A dijet Monte Carlo samples, generated with and without an underlying event. The sample without the underlying event was generated by turning off multiple parton interactions. The underlying event correction results in a decrease of the cross section varying from 22% at low p_T to 4% at high p_T; the hadronization correction increases the cross section by 13% at low p_T, and by 3.5% at high p_T. HERWIG 6.5 [22] provides consistent results on the hadronization corrections, but predicts smaller underlying event energy; the difference in the underlying event correction which is about 13% at low p_T and decreases with increasing p_T is taken as the underlying event correction uncertainty. In previous measurements at the Tevatron [1, 9], the hadronization corrections were not applied to the data. The inclusive jet cross section is shown in Figure 1 and Table I lists the cross sections with the statistical and systematic uncertainties at the hadron and parton levels. Also included in Table I are the explicit factors applied to the hadron level cross section to obtain the parton level cross section. The experimental and theoretical jet cross sections are obtained by averaging over the transverse momentum bins.

Current NLO theoretical predictions for inclusive jet production exist only at the parton level, for which the final state consists only of 2 or 3 partons [23–25]. For our comparisons with theory we use the calculation of EKS [23]. The ratio of the inclusive jet cross section, corrected to the parton level, to the NLO QCD predictions using the CTEQ6.1M PDF's is shown in Figure 2. The Midpoint jet algorithm has been applied to the 2 or 3 partons in the final state of the EKS calculation. In order to mimic the properties of the splitting/merging step, present at the experimental level but not at the NLO parton level, a parameter R_{sep} with a value of 1.3, has been introduced [26]. Two partons are clustered within the same jet if (1) they are within R_{cone} (0.7 for this measurement) of the jet centroid and (2) within $R_{sep} \times R_{cone}$ of each other. The use of $R_{sep} = 1.3$ results in a reduction of the theoretical cross section prediction by approximately 5%, independent of jet transverse momentum. In the EKS predictions, the renormalization and factorization scales (μ_R and μ_F) have both been set to $p_T^{jet}/2$. Using a scale of p_T^{jet} ($2p_T^{jet}$) rather than $p_T^{jet}/2$ leads to a theoretical prediction for the jet cross section lower by approximately 10% (20%) over the entire p_T range and a larger χ^2 in the global PDF fits [6]. The gluon distribution has been determined in the global fits, primarily by the Tevatron Run I jet data, using a renormalization and factorization scale of $p_T^{jet}/2$. Thus, for self-consistency, this scale should be used in the NLO comparisons.

We show in Figure 2 the experimental uncertainties for the inclusive jet cross section and the theoretical uncertainties estimated from the 40 CTEQ6.1M error PDF's [6]. The PDF uncertainty is the dominant theoretical uncertainty for most of the transverse momentum range. The correction for underlying event and hadronization is model dependent. The error associated with this correction is added in quadrature to the total experimental error and shown in Figure 2 as the outer shaded band. The data are in good agreement with the NLO QCD predictions.

It is important to emphasize that the CTEQ6.1M gluon density is already "enhanced" at high x and so automatically leads to a larger prediction for the jet cross section than older PDFs such as CTEQ5M. Also shown in Figure 2 is the prediction using the latest PDF set from the MRST group [8]. The MRST2004 PDF's also contain an enhanced higher x gluon, leading to better agreement with the CDF jet measurement.

In conclusion, we have measured the inclusive jet cross section in the range $61 < p_T < 620$ GeV/c using an improved iterative cone clustering algorithm, Midpoint. The new measurement extends the jet transverse momentum range over previous measurements at the Tevatron by about 150 GeV/c. The data are well described by NLO QCD predictions using CTEQ6.1M PDF's, within the theoretical (PDF) and experimental uncertainties. Inclusion of these data in future global PDF fits will provide further constraints on the gluon distribution at large x.

We thank the Fermilab staff and the technical staffs of the participating institutions for their vital contributions. This work was supported by the U.S. Department of Energy and National Science Foundation; the Italian Istituto Nazionale di Fisica Nucleare; the Ministry of Education, Culture, Sports, Science and Technology of Japan; the Natural Sciences and Engineering Research Council of Canada; the National Science Council of the Republic of China; the Swiss National Science Foundation; the A.P. Sloan Foundation; the Bundesministerium für Bildung und Forschung, Germany; the Korean Science and Engineering Foundation and the Korean Research Foundation; the Particle Physics and Astronomy Research Council and the Royal Society, UK; the Russian Foundation for Basic Research; the Comisión Interministerial de Ciencia y Tecnología, Spain; in part by the European Community's Human Potential Programme under contract HPRN-CT-2002-00292; and the Academy of Finland.

[1] CDF Collaboration, F. Abe *et al.*, Phys. Rev. Lett. **77**, 438 (1996), hep-ex/9601008.

[2] CDF Collaboration, T. Affolder *et al.*, Phys. Rev. D **64**, 032001 (2001), hep-ph/0102024.

[3] H.L. Lai *et al.*, Phys. Rev. D **55**, 1280 (1997), hep-ph/9606399.

[4] J. Huston *et al.*, Phys. Rev. Lett. **77**, 444 (1996), hep-ph/9511386.

[5] H.L. Lai *et al.*, Eur. Phys. J. **C12**, 375 (2000), hep-ph/9903282.

[6] J. Pumplin *et al.*, JHEP **0207**, 012 (2002), hep-ph/0201195.

[7] D. Stump *et al.*, JHEP **0310**, 046 (2003), hep-ph/0303013.

[8] A.D. Martin *et al.*, Phys. Lett. B **604**, 61 (2004), hep-ph/0410230.

[9] DØ Collaboration, B. Abbot *et al.*, Phys. Rev. Lett., **82**, 2451 (1999), hep-ex/9807018.

[10] We use a cylindrical coordinate system with the z coordinate along the proton beam direction and $z = 0$ at the center of the detector, the azimuthal angle ϕ, and the polar angle θ usually expressed through the pseudo-rapidity $\eta = -\ln\tan(\theta/2)$. The rapidity y is defined as $y = -1/2\ln((E+p_Z)/(E-p_Z))$ where E denotes the energy and p_Z is the momentum component along z.

[11] G. Flanagan, Ph.D. Thesis, Michigan State University (2005), FERMILAB-FN-0775-E.

[12] G.C. Blazey *et al.*, *"Run II Jet Physics: Proceedings of the Run II QCD and Weak Boson Physics Workshop"*, hep-ex/0005012.

[13] J.E. Huth *et al.*, *"Proceedings for Research Directions For the Decade: Snowmass 1990, July 1990"*, Ed. E.L. Berger (World Scientific, Singapore, 1992) p. 134.

[14] CDF Collaboration, D. Acosta *et al.*, Phys. Rev. D **71**, 032001 (2005), hep-ex/0412071.

[15] E. Gerchtein and M. Paulini, eConf **C0303241**, TUMT005 (2003), physics/0306031.

[16] G. Grindhammer, M. Rudowicz and S. Peters, Nucl. Instrum. Methods. and Phys. Res. A **290**, 469 (1990).

[17] A. Bhatti *et al.*, Nucl. Instrum. Methods. and Phys. Res. A, to be submitted, hep-ex/0510047.

[18] T. Sjöstrand *et al.*, Comput. Phys. Commun. **135**, 238 (2001), hep-ph/0010017; hep-ph/0108264.

[19] R. Field, presented at *Fermilab ME/MC Tuning Workshop*, Fermilab, October 4, 2002.

[20] CDF Collaboration, D. Acosta *et al.*, Phys. Rev. D **71**, 112002 (2005), hep-ex/0505013.

[21] The final state stable particles in Monte Carlo generators refer to colorless particles having a lifetime greater than approximately 10^{-11} s

[22] G. Corcella *et al.*, J. High Energy Phys., **0101**, 010 (2001), hep-ph/0011363; hep-ph/0210213;

[23] S.D. Ellis, Z. Kunszt and D.E. Soper, Phys. Rev. Lett. **64**, 2121 (1990).

[24] W.T. Giele, E.W.N. Glover and D.A. Kosower, Phys. Rev. Lett. **73**, 2019 (1994), hep-ph/9403347.

[25] Z. Nagy, Phys. Rev. Lett. **88**, 122003 (2002), hep-ph/0110315; Phys. Rev. D **68**, 094002 (2003), hep-ph/0307268.

[26] S.D. Ellis, J. Huston and M. Tonnesmann, eConf **C010630**, P513 (2001), hep-ph/0111434.

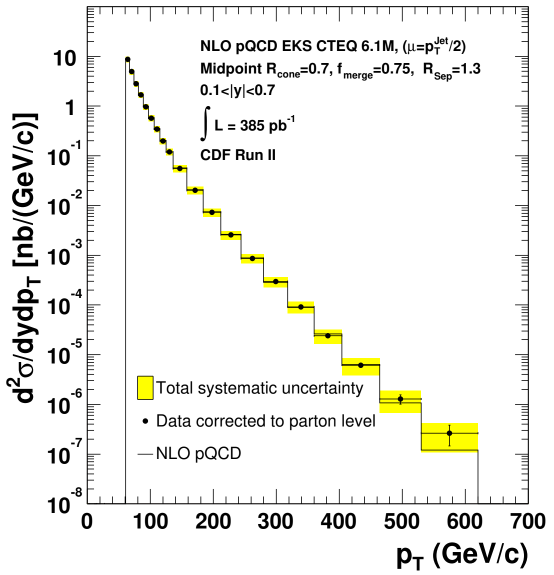

FIG. 1: *The measured inclusive jet differential cross section corrected to the parton level compared to the NLO pQCD prediction of the EKS calculation using CTEQ6.1M.*

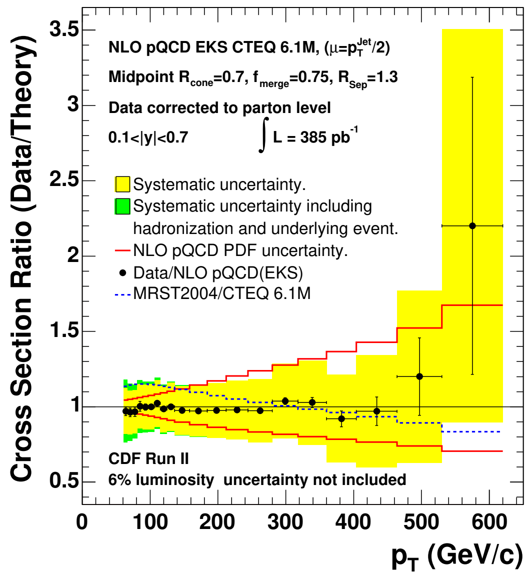

FIG. 2: *The ratio of the data corrected to the parton level over the NLO pQCD prediction of the EKS calculation using CTEQ6.1M. Also shown are the experimental systematic errors and the theoretical errors from the PDF uncertainty. The ratio of MRST2004/CTEQ6.1M is shown as the dashed line. An additional 6% uncertainty on the determination of the luminosity is not shown.*

TABLE I: *Results for the inclusive jet cross section corrected to the hadron level, $d^2\sigma^{hadron}/dp_T dy$, and to the parton level, $d^2\sigma^{parton}/dp_T dy$ are shown for each bin together with the statistical (first) and systematic (second) errors. C^{UE} is the underlying event correction and C^{Had} is the hadronization correction which is applied to the data. The total hadron to parton level correction is given by $C^{h\to p} = C^{UE} \cdot C^{Had}$. There is an additional 6% luminosity uncertainty.*

p_T (GeV/c)	$\frac{d^2\sigma^{hadron}}{dp_T dy}$ (nb/(GeV/c))	C^{UE}	C^{Had}	$\frac{d^2\sigma^{parton}}{dp_T dy}$ (nb/(GeV/c))
61-67	$(8.77 \pm 0.25 \pm 1.37) \times 10^0$	0.781	1.138	$(7.79 \pm 0.23 \pm 1.67) \times 10^0$
67-74	$(4.93 \pm 0.14 \pm 0.74) \times 10^0$	0.804	1.123	$(4.46 \pm 0.13 \pm 0.88) \times 10^0$
74-81	$(2.82 \pm 0.86 \pm 0.42) \times 10^0$	0.825	1.111	$(2.58 \pm 0.08 \pm 0.48) \times 10^0$
81-89	$(1.69 \pm 0.54 \pm 0.25) \times 10^0$	0.842	1.101	$(1.56 \pm 0.05 \pm 0.27) \times 10^0$
89-97	$(9.68 \pm 0.19 \pm 1.43) \times 10^{-1}$	0.857	1.092	$(9.07 \pm 0.19 \pm 1.54) \times 10^{-1}$
97-106	$(5.70 \pm 0.74 \pm 0.85) \times 10^{-1}$	0.871	1.085	$(5.38 \pm 0.08 \pm 0.90) \times 10^{-1}$
106-115	$(3.45 \pm 0.49 \pm 0.53) \times 10^{-1}$	0.883	1.078	$(3.28 \pm 0.05 \pm 0.54) \times 10^{-1}$
115-125	$(2.00 \pm 0.29 \pm 0.31) \times 10^{-1}$	0.893	1.073	$(1.91 \pm 0.03 \pm 0.32) \times 10^{-1}$
125-136	$(1.19 \pm 0.18 \pm 0.19) \times 10^{-1}$	0.902	1.068	$(1.15 \pm 0.02 \pm 0.19) \times 10^{-1}$
136-158	$(5.56 \pm 0.60 \pm 0.93) \times 10^{-2}$	0.914	1.062	$(5.39 \pm 0.07 \pm 0.92) \times 10^{-2}$
158-184	$(2.03 \pm 0.22 \pm 0.36) \times 10^{-2}$	0.926	1.056	$(1.98 \pm 0.03 \pm 0.35) \times 10^{-2}$
184-212	$(7.28 \pm 0.86 \pm 1.35) \times 10^{-3}$	0.936	1.051	$(7.16 \pm 0.10 \pm 1.34) \times 10^{-3}$
212-244	$(2.58 \pm 0.32 \pm 0.51) \times 10^{-3}$	0.943	1.047	$(2.55 \pm 0.04 \pm 0.51) \times 10^{-3}$
244-280	$(8.60 \pm 0.13 \pm 1.85) \times 10^{-4}$	0.949	1.043	$(8.51 \pm 0.13 \pm 1.83) \times 10^{-4}$
280-318	$(2.96 \pm 0.06 \pm 0.71) \times 10^{-4}$	0.953	1.041	$(2.94 \pm 0.01 \pm 0.70) \times 10^{-4}$
318-360	$(9.18 \pm 0.29 \pm 2.49) \times 10^{-5}$	0.956	1.039	$(9.11 \pm 0.30 \pm 2.47) \times 10^{-5}$
360-404	$(2.41 \pm 0.14 \pm 0.76) \times 10^{-5}$	0.958	1.037	$(2.40 \pm 0.14 \pm 0.76) \times 10^{-5}$
404-464	$(6.16 \pm 0.60 \pm 2.36) \times 10^{-6}$	0.960	1.036	$(6.12 \pm 0.60 \pm 2.35) \times 10^{-6}$
464-530	$(1.29 \pm 0.28 \pm 0.62) \times 10^{-6}$	0.961	1.035	$(1.28 \pm 0.28 \pm 0.61) \times 10^{-6}$
530-620	$(2.64 \pm 1.18 \pm 1.57) \times 10^{-7}$	0.961	1.034	$(2.63 \pm 1.18 \pm 1.56) \times 10^{-7}$